The Climatology of Synoptic-Scale Ascent over Western North America: A Perspective on Storm Tracks

NEIL P. LAREAU AND JOHN D. HOREL

Department of Atmospheric Sciences, University of Utah, Salt Lake City, Utah

(Manuscript received 10 August 2011, in final form 5 December 2011)

ABSTRACT

The position and variability of storm tracks across western North America are examined during the October–April cool seasons spanning 1989–2010. The location and intensity of storms are represented by strong synoptic-scale ascent, which is diagnosed by the alternative balance omega equation applied to ECMWF Re-Analysis Interim data. This dynamically filtered method removes poorly resolved updrafts arising from subsynoptic-scale phenomena such as convection and mountain waves. The resulting vertical motions are illustrated for the case of a strong storm traversing the western United States.

Summary statistics of synoptic-scale ascent are compiled over months, seasons, and the entire 21-yr period. Locations exhibiting high mean values of ascent are deemed to represent storm tracks. The climatological-mean storm track exhibits a sinusoidal shape across the eastern Pacific and western North America. The composite evolution of strong storms moving along specific segments of the storm track show regional differences (e.g., storms poleward of 50°N tend to result from progressive low-amplitude troughs progressing through the mean planetary ridge, while storms over the western United States are initiated by digging troughs that temporarily suppress the mean ridge).

Seasonal shifts in the storm track are pronounced and exhibit coherent regional patterns. Interannual variations in synoptic-scale ascent indicate meridional shifts in position as well as changes in the degree of amplification within the dominant sinusoidal storm track. These changes in structure are related to the phase of ENSO: El Niño (La Niña) winters favor zonal (amplified) and southern (northern) storm tracks.

1. Introduction

Storm tracks, or regions where the synoptic-scale transient eddy activity is locally most prevalent and intense (Glickman 2000), are of global importance. The location and intensity of storms occurring within these preferred pathways play a major role in the earth's climate system by redistributing heat, momentum, and moisture. They also strongly affect the distribution of midlatitude cool-season precipitation. Owing to their profound importance, the primary Northern Hemisphere storm tracks have been studied in depth for better than half a century (Petterssen 1956; Klein 1957; Blackmon 1976; Sickmöller et al. 2000; Hoskins and Hodges 2002, hereafter HH02; Wettstein and Wallace 2010).

Storm tracks are also of manifest regional importance. The occurrence and progression of storms across western North America have a significant impact on the region's hydrologic cycle during the cool season (October–April), particularly in terms of the development of mountain snowpacks (Changnon et al. 1993; Cayan 1996; Serreze et al. 1996). Interannual variations in the location and intensity of storms over western North America contribute to significant societal impacts ranging from the frequency of floods to the availability of water for agriculture and recreational pursuits (Cayan 1996; Dettinger et al. 1998). From a climate change perspective, potential systematic shifts in the storm track across the region may have far reaching consequences (Mote et al. 2005; Mote 2006; Bengtsson et al. 2006; Pierce et al. 2008).

However, there is no consensus for the climatological location, seasonality, and variability of the storm tracks across western North America (Fig. 1).This ambiguity results from the complex terrain–flow interactions over the region, which in turn has led to disparate methodologies to identify storms (Table 1). While some authors

Corresponding author address: Neil Lareau, Department of Atmospheric Sciences, University of Utah, 135 South 1460 East, Room 819, Salt Lake City, UT 84112.
E-mail: neil.lareau@utah.edu

DOI: 10.1175/MWR-D-11-00203.1

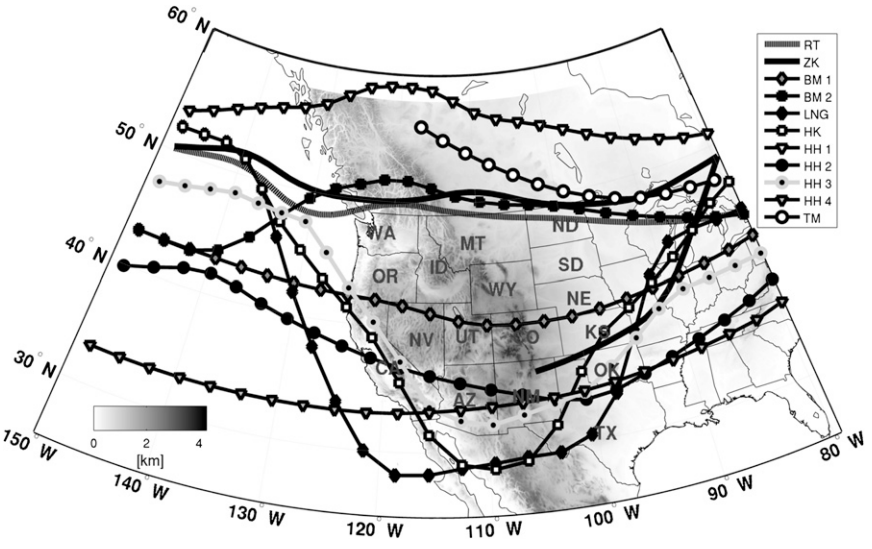

FIG. 1. Comparative storm-track climatologies (assorted lines) and the topography (gray shading) for western North America. Storm-track climatology abbreviations shown in the legend and study methodology are detailed in Table 1. All storm tracks are visual estimates from published figures.

simply omit the region from storm-track climatologies (Wernli and Schwierz 2006; Raible et al. 2008), the most common approach is to identify and track surface cyclones (Petterssen 1956; Klein 1957; Reitan 1974; Zishka and Smith 1980; Whittaker and Horn 1981; HH02; Jeglum et al. 2010). This approach presumes that the coherent link between cyclones and oceanic storm tracks also applies over western North America despite the substantive effect that mountains have on the structure of baroclinic waves (Davis 1997; Davis and Stoelinga 1999). The resulting storm-track climatologies depict differing preferred cyclone locations (Reitan 1974; Jeglum et al. 2010), discontinuous pathways, and multiple regional maxima (Jeglum et al. 2010), or even a complete absence of cyclones (HH02) within interior western North America.

In contrast, storm-track studies that examine baroclinic eddies within the mid- to upper troposphere tend to indicate more continuous pathways across the domain (Blackmon 1976; Lefevre and Nielsen-Gammon 1995; HH02; Hakim 2000, hereafter HK00). However, even among the mid- to upper-tropospheric storm climatologies

TABLE 1. Details and abbreviations for storm-track climatologies displayed in Fig. 1.

Study	Abbreviation	Method	Season/years
Reitan (1974)	RT	Mean sea level pressure (MSLP) cyclones	Jan/1951–70
Zishka and Smith (1980)	ZK	MSLP cyclones	Jan/1950–77
Blackmon (1976)	BM 1	500-hPa heights, 2.5–6-day bandpass variance for medium waves	Year/1963–72
—	BM 2	500-hPa heights, 1–2-day bandpass variance for short waves	—
Lefevre and Nielsen-Gammon (1995)	LNG	500-hPa trough tracking, Eulerian centripetal acceleration (geostrophic curvature vorticity flux)	Year/1969–88
Hakim (2000)	HK00	500-hPa geostrophic cyclonic-relative vorticity density	Dec–Feb/1957–89
Hoskins and Hodges (2002)	HH02 1	MSLP 2–6-day bandpass variance	Dec–Feb/1979–2000
—	HH02 2	500-hPa omega, 2–6-day bandpass variance	—
—	HH02 3	250-hPa cyclonic-relative vorticity feature density	—
—	HH02 4	2-PVU 2–6-day bandpass variance	—
Thomas and Martin (2007)	TM	MSLP	Oct–Mar/1986–2001

summarized in Fig. 1, the latitude of the mean storm track over western North America varies from 30° to 55°N and spatial distributions range from approximately zonal (Blackmon 1976; HH02) to amplified sinusoidal configurations (Lefevre and Nielsen-Gammon 1995; HK02). As summarized by HH02, these differences are not unexpected, as each approach tends to emphasize different physical processes of relevance to storm tracks.

In addition, seasonal and interannual variations in the storm tracks across the region are not particularly well understood. Myoung and Deng (2009) document interannual variability in cyclone occurrence and regional precipitation along the west coast of North America that is dominated by a north–south dipole with links to the El Niño–Southern Oscillation (ENSO) phenomenon. However, it is not clear from their study if variations in the number of cyclones along the coast reflect the variability of the storm tracks throughout western North America. Most other storm-track investigations focus separately on variability within the primary Pacific and Atlantic oceanic storm tracks (Lau 1988; Wettstein and Wallace 2010; Athanasiadis et al. 2010) leaving variations in storminess across western North America less studied.

The goal of this paper is to document the climatological distribution and variability of storms across western North America. To do so, we will first demonstrate a novel methodology for assessing storm tracks, which is appropriate for mountainous regions and employs synoptic-scale ascent as a physically significant measure of storm location and intensity (section 2). In section 3a, the performance of this metric is demonstrated for the case of a vigorous synoptic-scale disturbance traversing the Intermountain West. We subsequently expand the analysis and apply our technique to document the climatological distribution, seasonal cycle, and interannual variability of cool season (October–April) storms from 1989 to 2010 (sections 3b–e). Comparison of these results to previous storm-track climatologies and conclusions follow in section 4.

2. Data and methods

a. Data

The European Centre for Medium-Range Weather Forecasts (ECMWF) Re-Analysis (ERA)-Interim data are used in this study (Dee et al. 2011). The ERA-Interim is produced using the ECMWF Integrated Forecasting System configured with a T255 triangular truncation and 60 vertical levels. It uses a four-dimensional variational data assimilation system that ingests observations within a 12-h window around the analysis time. The postprocessed data used in this study are available at 6-h intervals (0000, 0600, 1200, and 1800 UTC) on 37 isobaric levels with a horizontal resolution of 1.5° (~165 km at 45°N). Our investigation focuses on five isobaric levels (700, 600, 500, 400, and 300 hPa), although additional levels were used to evaluate the methodology. The study domain is bounded by 22°–56°N and 80°–150°W, covering most of western North America and adjacent portions of the eastern Pacific Ocean. The analysis period spans 21 boreal cool seasons (October–April) during 1989/90–2009/10.

b. Methods

1) The alternative balance (AB) omega equation

Synoptic-scale ascent is used to characterize the location and intensity of storm systems while excluding poorly resolved subsynoptic-scale motions. We choose this field over more conventional storm-track variables, for example, local minima in sea level pressure (Petterssen 1956) or bandpass-filtered geopotential height variance (Blackmon 1976) because of its direct dynamical, physical, and practical significance. Durran and Snellman (1987) note "one forecast variable which has a very pronounced effect on the weather is the vertical velocity. Sustained upward motion produces condensation and precipitation, destabilization of the lapse rate, and intensification of midlatitude cyclones." Although direct evaluation of vertical motions from numerical model output (such as the postprocessed ERA-interim analyses) is possible (e.g., HH02), the recurrence of mountain waves proximal to the coarsely resolved model topography as well as vertical motions resulting from incomplete or inappropriate physical parameterizations are impediments to this approach.

An alternative method to diagnose synoptic-scale vertical motion follows the quasigeostrophic (QG) dynamical framework (Hoskins and Pedder 1980; Holton 2004; Martin 2006), which is routinely employed for case studies of high-impact weather events (Martin 2007; West and Steenburgh 2010). Yet, diagnosing QG synoptic-scale vertical motions cumulatively over many storms or longer climatological time spans is less common (Deveson et al. 2002; Thomas and Martin 2007).

In this study we employ the **Q**-vector form of the omega equation (Hoskins et al. 1978) to infer synoptic-scale ascent–descent of $O(0.1\ \text{Pa s}^{-1}; 1\ \text{cm s}^{-1})$. However, following Davies-Jones (1991, 2009), we replace the geostrophic wind by the nondivergent wind in the formulation of the alternative balance (AB) **Q** vector. The AB form of the omega equation provides an approximation to the vertical velocity of the primitive

equations while maintaining the diagnostic form of its QG counterpart. A significant benefit of the AB approach is that vertical velocities are not over (under) estimated in regions of strong cyclonic (anticyclonic) curvature as with QG omega.

To formulate the AB omega equation, the nondivergent wind is obtained by decomposing the ERA-Interim isobaric winds into their nondivergent and irrotational components. The nondivergent portion is given by

$$\mathbf{V}_\psi = (u_\psi, v_\psi), \quad u_\psi = -\frac{\partial \psi}{\partial y}, \quad v_\psi = \frac{\partial \psi}{\partial x}, \tag{1}$$

where the streamfunction ψ is obtained by inverting

$$\nabla^2 \psi = \zeta = \frac{\partial v}{\partial x} - \frac{\partial u}{\partial y} \tag{2}$$

(Krishnamurti and Bounoua 1996) and ζ is the ERA-Interim vertical component of relative vorticity. The AB **Q**-vector form of the omega equation is then

$$\sigma \nabla_p^2 \omega + f_0^2 \frac{\partial^2}{\partial p^2} \omega = -2 \nabla_P \cdot \mathbf{Q}_{\mathrm{AB}} \tag{3}$$

(Davies-Jones 1991), where ω is the pressure coordinate vertical velocity (Pa s^{-1}), f_0 is the Coriolis parameter, and σ is the static stability parameter. $\mathbf{Q}_{\mathrm{AB}}$ is defined by

$$\mathbf{Q}_{\mathrm{AB}} = \left[\frac{-R}{P} \left(\frac{\partial \mathbf{V}_\psi}{\partial x} \right) \cdot \nabla_p T, \quad \frac{-R}{P} \left(\frac{\partial \mathbf{V}_\psi}{\partial y} \right) \cdot \nabla_p T \right], \tag{4}$$

where T is the temperature, R is the dry air gas constant, and P is the pressure level. The quantity $\mathbf{Q}_{\mathrm{AB}}$ represents the vector rate of change of the horizontal temperature gradient across a fluid parcel traveling along a trajectory defined by the nondivergent wind (Keyser et al. 1988) and its convergence can be used to infer synoptic-scale ascent.

To estimate the distribution of omega over the study domain, (3) must be integrated in the horizontal and vertical subject to appropriate boundary conditions. We assume $\omega = 0$ at the lateral boundaries and limit the integration to five midtropospheric levels (700, 600, 500, 400, and 300 hPa) with $\omega = 0$ at 850 and 200 hPa. The lower boundary for which omega is diagnosed (700 hPa) resides above the elevation of nearly all topographic features in the domain, which helps to reduce vertical motions arising from terrain–flow interactions. Omega was calculated using 31 ERA-Interim pressure levels (850–1 hPa) for selected cases and the salient synoptic-scale omega features were found to be adequately resolved by the analysis limited to 5 levels; this restriction to 5 levels also served to make the analysis computationally efficient. In addition, Durran and Snellman (1987) and Clough et al. (1996) note that the omega distribution arrived at by the integration of (3) is dominated by longwave forcing aloft, insensitive to low-altitude forcing, and maximized in the midtroposphere (e.g., near 500 hPa). Finally, the relatively coarse grid (1.5°) of the postprocessed ERA-Interim data diminishes the impact of subsynoptic-scale features, such as mountain waves.

The vertical motions diagnosed from the integration of (3) are sensitive to latitude and the specification of static stability (Clough et al. 1996); ascent is reduced in locations of high stability and latitude for a given magnitude of the right-hand side of (3). In this study, σ is evaluated from the differences in ERA-Interim temperature between pressure levels and any absolute instabilities in the data are removed. Since diabatic heating is neglected in our version of the AB omega equation, the strong positive feedback on ascent is not present where condensation is taking place.

2) Eulerian storm-track statistics

The climatological distribution of synoptic-scale ascent diagnosed from the integration of (3) is summarized by three Eulerian statistics. Collectively, these three interrelated metrics reflect the statistical prevalence and local intensity of ascent, which we argue is synonymous with the definition of storm tracks (Glickman 2000).

The mean ascent, $\overline{\omega}$, at a particular grid point is defined here as

$$\overline{\omega} = \frac{1}{n} \sum_{i=1}^{n} \beta_i \omega_i^m, \tag{5}$$

where the summation is over all 6-h increments (n) in a given observation period. The maximum ascent (ω^m) is the minimum omega of the five values in the column, which in practice typically occurs between 600 and 400 hPa. When ω^m is less than -0.1 Pa s^{-1} (greater than $\sim$1 cm s^{-1}), the event parameter β equals 1 at that grid point; otherwise, β is 0. The use of β defines a storm footprint by excluding descending motions and small ascending motions from the climatological statistics. The threshold value for β was established based on typical scaling arguments for synoptic-scale vertical motion and was also found to be the $\sim$90th percentile of 500-hPa ascending motions within our 21-yr sample. The appropriateness of this threshold has been examined through subjective evaluations of season-long animations of ascending motion at 6-h intervals. Altering this

threshold does not significantly alter the climatological storm-track structures presented in section 3b.

Within any sample, the mean ascent $\overline{\omega}$ can be viewed as the product of how often ascent takes place and the average magnitude of ascent when it happens. Hence, the mean ascent frequency f or the percentage of time a grid point experiences ascent greater than the threshold value β, is given by

$$f = \left(\frac{1}{n}\sum_{i=1}^{n}\beta_i\right)100, \tag{6}$$

while the average ascent magnitude is

$$\overline{\omega^*} = \frac{1}{\sum_{i=1}^{n}\beta_i}\sum_{i=1}^{n}\beta_i\omega_i^m. \tag{7}$$

The sample size n can be restricted to a single storm, expanded to cover a complete season, or denote the entire 21-yr cool-season climatological record.

3. Results

a. Case study

The purpose of this section is to demonstrate the characteristics of ascent derived from the AB omega diagnostic during the ''Tax Day Storm'' (West and Steenburgh 2010, hereafter WS10). This storm traversed the western United States on 14–16 April 2002 and brought damaging winds, blowing dust, extreme low pressure, sharp frontal passages, and heavy precipitation across much of Nevada, Utah, Idaho, and Wyoming. While WS10 provide considerable insight into the complex terrain–flow interactions, mesoscale frontal structures, and diabatic heating during this event, we focus on the overall temporal and spatial evolution of the storm system as summarized by synoptic-scale ascent.

A positively tilted trough at 500 hPa is approaching the West Coast of the United States at 1800 UTC 14 April 2002 (Fig. 2a). The maximum ascent, ω^m, as diagnosed by the AB omega equation is centered over the western seaboard and situated downstream of the trough axis. The footprint of the Tax Day Storm is defined by the -0.1 Pa s^{-1} ($\sim$1 cm s^{-1}) contour (dashed white outlines in the top panels of Fig. 2). The event parameter, β, at each grid point is set to one within the footprint and set to zero elsewhere. (For the climatological statistics in the next section, β is set to 1 anywhere the threshold is exceeded, which would include the areas in the top-right region of the domain in this instance.) Infrared satellite imagery indicates cold cloud tops over much of Utah, Colorado, and Wyoming with warmer clouds associated with a weakening surface cyclone offshore from Canada. Radar returns are present over portions of Idaho and Montana associated with convection near a surface baroclinic trough (WS10). Notably, few clouds and no significant precipitation features are found within the ascent maximum associated with the Tax Day Storm.

The trough digs to the southeast over the next 6 h and vigorous synoptic-scale ascent is centered over northern California (Fig. 2b). Precipitation, including some strong convection in Montana, is not associated with regions of strong synoptic-scale ascent as deduced from this diagnostic. The trough shifts onshore and amplifies by 0600 UTC and is accompanied with a broad storm footprint with the strongest ascent of the event centered near the California–Nevada border (Fig. 2c). Nascent low- and midlevel clouds are found within the region of rising motion, although precipitation remains spotty and focused along the preexisting surface frontal zone (WS10). At 1200 UTC, the eastward progression of the trough has slowed with the trough axis assuming a slight negative tilt (Fig. 2g). Strong ascent occurs over central and southeastern Nevada, but also in an arc to the northeast across portions of Utah, Idaho, and Wyoming. Deeper clouds and more widespread precipitation are evident coincident with regions of ascent. Precipitation becomes heavy and widespread within this same arc at 1800 UTC (Fig. 2h), although the synoptically forced ascent weakens considerably and two separate ascent maxima emerge over northeastern and southeastern Nevada, respectively. Ascent associated with the Tax Day Storm exhibits a further splitting and weakening by 0000 UTC 16 April (Fig. 2i). One ascent lobe progresses southeastward into northern Arizona, while the northern branch of ascent develops a new local maximum to the east of the continental divide.

The collocation of synoptic-scale ascent with clouds and precipitation is most apparent during the latter phases of the Tax Day Storm, while the lack of clouds earlier may reflect insufficient time for air parcels to reach saturation within the vigorous updrafts. Despite the absence of clouds, it is likely that the early phases of the storm play an important role in preconditioning air parcels through large-scale ascent, which may later contribute to cloud and precipitation processes both on synoptic and smaller scales. The strong ascent, cloud free or otherwise, also alters the distribution of vorticity and mass within the lower troposphere. Between 0600 and 1800 UTC 15 April, strong synoptic-scale ascent and its associated column stretching interacts both with a lee trough downstream of the Sierra Nevada and a preexisting surface baroclinic trough over Nevada to initiate

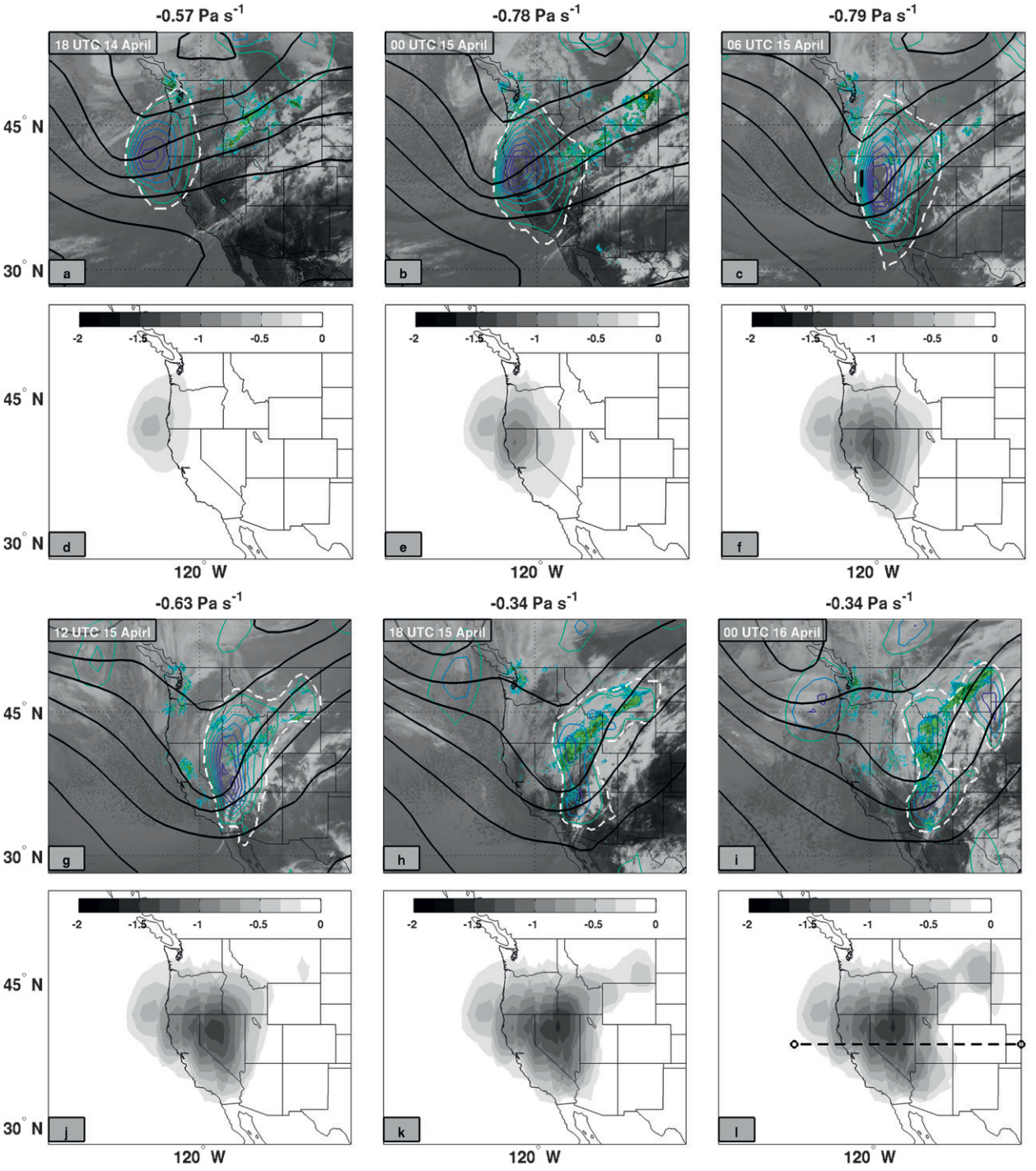

FIG. 2. The Tax Day Storm evolution from 1800 UTC 14 Apr–0000 UTC 16 Apr 2002. (a)–(f) Alternative balance (AB) minimum omega (colored contours for $\omega^m < -0.1$ Pa s^{-1}, interval 0.075 Pa s^{-1}), 500-hPa geopotential height (black contours, interval 100 m), infrared satellite imagery (gray shading), and composite base elevation (0.5°) radar reflectivity from ±10 min of the displayed time stamp. The storm footprint, or regions where the event parameter β is set to one is defined by the white dashed contour ($\omega^m = -0.1$ Pa s^{-1}). This contour is manually suppressed for regions unrelated to the Tax Day Storm. The strongest ascent (Pa s^{-1}) at each time is displayed at the top of each. (g)–(l) Accumulated AB minimum omega associated with the Tax Day Storm, shaded values (Pa s^{-1}) according to the color bar. The location, 39°N, of the cross section used in Fig. 3 is shown in (l).

a surface confluence zone, cyclogenesis, and later strong frontal contraction (WS10). As the cyclone progressed eastward, the second lowest sea level pressure on record was observed at Salt Lake City, Utah, at 2100 UTC 15 April (WS10).

The storm track for the Tax Day Storm is established by accumulating the maximum ascent ω^m within the storm footprint at each successive time step (Fig. 2, bottom panels). As before, the accumulation here is restricted to within the footprint of this specific storm. Despite the distinct edges due to the discrete 6-h time steps, it is apparent from Fig. 2 that the storm had its greatest ascent in the swath stretching from northern California, across Nevada, and extending through portions of Utah, Idaho, and Wyoming with a second branch (associated with the southern ascent lobes emerging around 1800 UTC 15 April) extending into Arizona. The strongest sensible weather impacts from the Tax Day Storm were observed in these regions (WS10).

Figure 3 contrasts the analyzed omega from the ERA-Interim with the synoptic-scale AB omega diagnosed from the integration of (3) along 39°N during the Tax Day Storm. Not surprisingly, the distribution of the AB omega is smoother and tends to be more closely associated with the synoptic-scale disturbance than the ERA-Interim omega. During the lifetime of the storm, the AB omega exhibits a quasi-symmetric dipole about the downward deflection of the dynamic tropopause [2 potential vorticity unit (PVU; 1 PVU = 10^{-6} K m^2 kg^{-1} s^{-1}) contour in Fig. 3] and tends to maximize between 400 and 600 hPa. In contrast, the ERA-Interim omega frequently displays significant vertical motion well removed from the upper-level cyclonic potential vorticity anomaly, for example, the near-surface couplet of up- and downdrafts likely induced by the flow over the terrain near 106°W (Figs. 3e,f, terrain in Fig. 3g). By filtering these types of motions, the AB omega equation is able to isolate the motions associated with the transient synoptic-scale system. However, the synoptic-scale omega tends to be weaker than its ERA-Interim counterpart. The weaker AB omegais due to the cumulative effects of neglecting the forcing for ascent by diabatic heating and the coarseness of the post processed ERA-Interim grid that limits the intensity of resolved gradients in the temperature and wind, and thus the **Q** vector and its convergence (Elbern et al. 1998).

Reinforced by inspection of additional case studies and animations of synoptic-scale omega throughout the entire 21-yr period, we conclude that the AB omega diagnostic is a useful approach to define the progression and intensity of synoptic-scale storms across western North America. Hence, we now turn to documenting the climatological distribution of storms, which we consider in the following section.

b. Long-term means

In this section, we summarize the characteristics of synoptic-scale ascent over western North America and the adjacent regions for the entire 21-yr (1989–2010) cool-season (October–April) period. Figure 4 shows the climatological distribution of mean ascent $\overline{\omega}$ over the study domain. Ascent is most frequent and intense within a sinusoidal band bounded by the -1 cPa s^{-1} ($\sim$0.1 cm s^{-1}) contour. This band and its centroid (determined as the meridional maxima in ascent after smoothing with a fifth-order Butterworth low-pass filter) are subsequently referred to as the primary storm track as they provide an Eulerian measure of the prevalence for ascent accompanying synoptic-scale storms. However, we emphasize that our primary storm track is not an indicator of the Lagrangian pathway of the ''mean storm'' and assumes its sinusoidal appearance as the result of connecting localized regions of high mean ascent.

The shape, maxima, and minima of $\overline{\omega}$ are closely related to the climatological mean 500-hPa geopotential height (black contours in Fig. 4). Ascent tends to be greatest (least) upstream (downstream) from the mean ridge axis over the Canadian Rockies and downstream (upstream) of the weak trough over the southwestern United States). For example, a pronounced maximum in ascent (A in Fig. 4) parallels the British Columbia (BC) coast immediately upstream from the mean ridge axis while infrequent and weak ascent (hence more frequent subsidence) occur downstream of the ridge over Alberta, Saskatchewan, and Montana. The greatest ascent anywhere in the domain, with mean ascent exceeding -2 cPa s^{-1} ($\sim$0.2 cm s^{-1}), is situated over Arizona just east of the weak mean trough found at these latitudes. The portion of the storm track that connects the coastal BC and Arizona maxima is found at the inflection point between the mean ridge to the north and trough to the south.

Strong ascent, including a local maximum over Oklahoma (C in Fig. 4), is also found in a broad northeasterly swath downstream of the Rocky Mountains and extending toward the Great Lakes. This northeasterly trend of the storm track may be due to the impact of the Rocky Mountains on jet stream orientation, mean-flow ascent anomalies, and near-surface baroclinicity (Brayshaw et al. 2009). The local maximum over Oklahoma is likely related to lee cyclones that mature to deeper baroclinic disturbances as they move downstream (Hobbs et al. 1996).

The frequency of occurrence of synoptic-scale ascent f exhibits a similar sinusoidal pattern and the primary storm track coincides with regions experiencing ascent more than 6% of the time (Fig. 5a). The stormiest locations (A and B in Fig. 5a) are prone to significant ascent approximately once every 10–11 days. The similarities

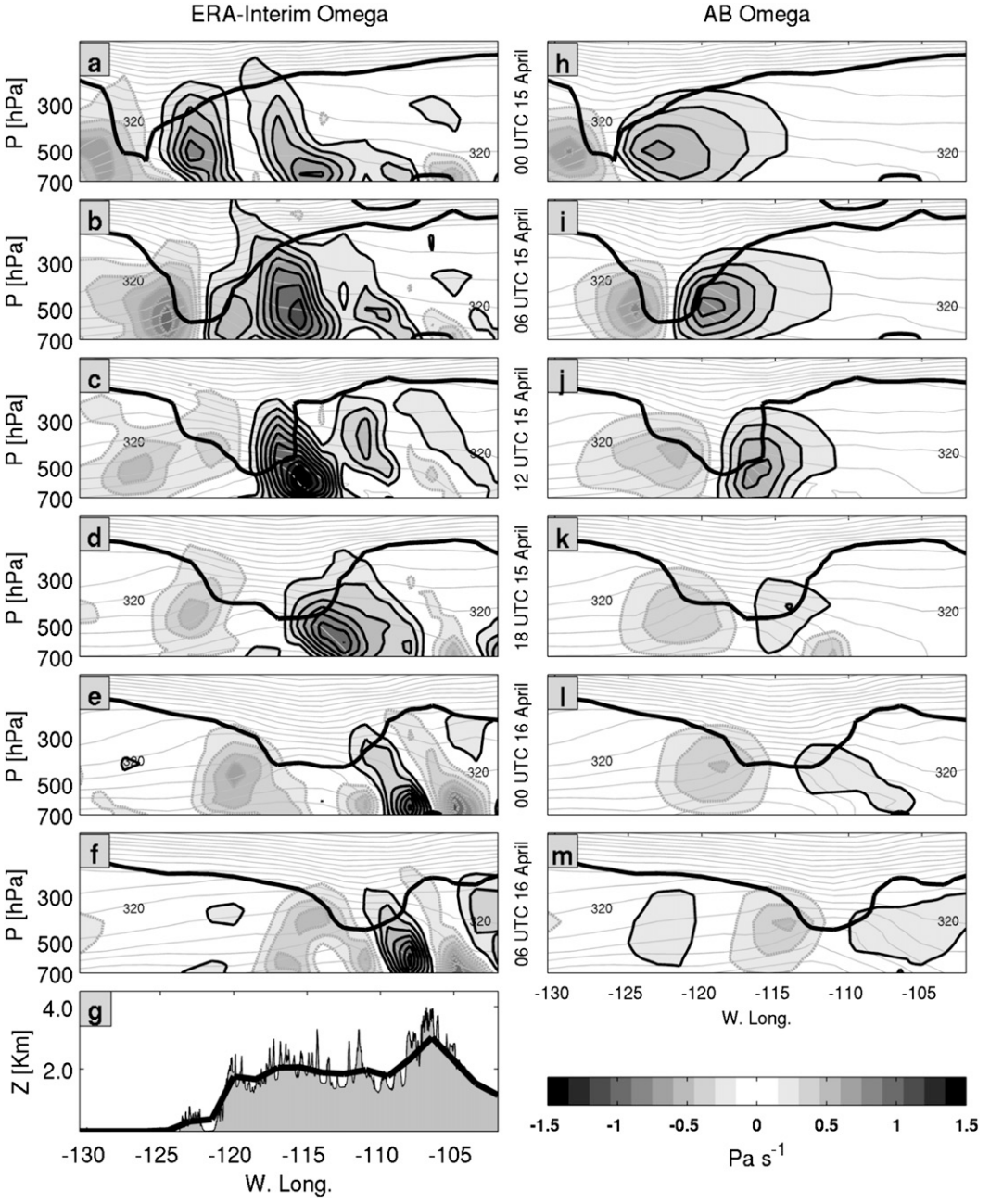

FIG. 3. Cross section, at 39°N, through the Tax Day Storm from 0000 UTC 15 Apr–0600 UTC 16 Apr 2002 at 6-h increments showing (a)–(f) omega from the ERA-Interim and (h)–(m) the AB omega equation. Ascent (descent) is shaded with black (gray) contours. The dynamic tropopause defined by 2 PVU is denoted by the heavy black lines. Potential temperature at an interval of 5 K (with the 320-K isotherm labeled for reference) is shown by the light gray lines. The terrain in (g) from the ERA-Interim (black line) and a high-resolution digital elevation model (gray shading) are shown for reference.

between Figs. 4 and 5a suggest that the location and embedded maxima of the primary storm track are largely a result of the frequency of occurrence of ascent events, or storms, with the magnitude of ascent during a particular event of secondary importance. However, because the mean ascent magnitude per event $\overline{\omega^*}$ tends to maximize near 35°N, the more southern portions of the storm track may be regarded as both a function of frequency and intensity (Fig. 5b). It should also be noted that the mean ascent maximizes at 500 hPa except over the lee slopes of

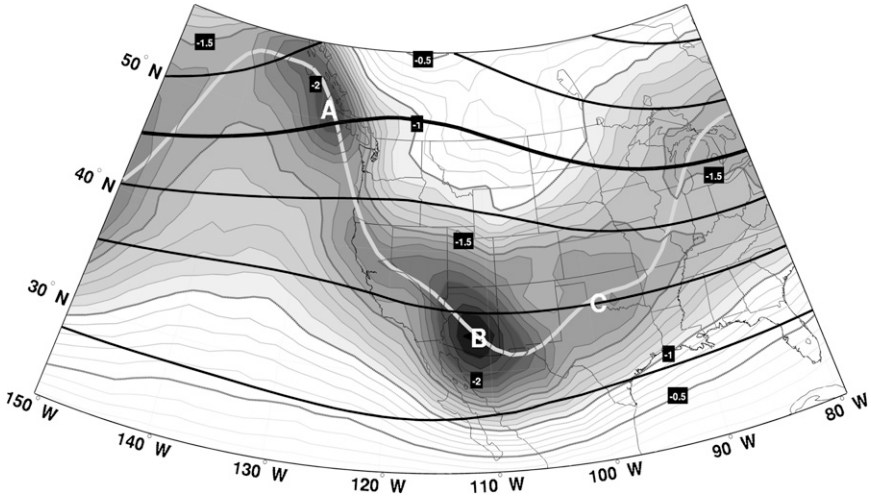

FIG. 4. Climatological mean synoptic-scale ascent, $\overline{\omega}$ (labeled at intervals of 0.5 cPa s^{-1}, dashed contours every 0.1 cPa s^{-1}, and shading below -1 cPa s^{-1}) during 21 cool seasons (October–April) 1989–2010. Shaded regions denote locations within the primary storm track and the solid gray line depicts the storm track centroid. Letters A–C denote locations of local ascent maxima. The climatological mean 500-hPa geopotential height is shown by solid black contours at an interval of 100 m with the 5500-m contour emphasized for reference.

the Rocky Mountains and south of ~28°N where it has a tendency to occur at 400 hPa (not shown).

Apparent in both Figs. 4 and 5a is a secondary (and much weaker) storm pathway near 52°N, which extends zonally from coastal BC through the mean ridge axis and east toward Lake Winnipeg before eventually merging with the primary storm track near the Great Lakes. This feature is robust in the climatology, appearing to varying degrees in all 21 individual cool seasons (not shown).

c. Storm-track composites

The composite storm motion and evolution along discrete segments of the storm track provides additional insight into the geographic distribution of ascent. The 500-hPa geopotential height and synoptic-scale ascent are compiled for the 105 (~5 yr^{-1}) strongest independent ascent events affecting representative regions along the storm track. The composite evolution begins 36 h prior to the storms arrival in the region of interest and terminates 24 h later. The resulting composite storms and accumulated ascent storm tracks are summarized in Fig. 6.

Strong composite ascent along coastal BC originates from a low-amplitude trough crossing the eastern Gulf of Alaska (Fig. 6a). Ascent incrementally increases along a southwest to northeast fetch as the storm approaches the coastline with its peak intensity just before landfall. As the trough moves onshore, it flattens and ascent diminishes. The weakened composite trough then continues to propagate eastward (not shown) through the climatological mean ridge and does not veer south along the Pacific Northwest coast as one might erroneously infer from the Eulerian storm track in Fig. 4.

A subset of eastward-moving coastal BC storms redevelop stronger ascent downstream from the Canadian Rockies over Alberta and Saskatchewan (Fig. 6b). It is these diminutive waves that form the weak northern storm track across southern Canada apparent in Figs. 4 and 5a. Storms along this track also tend to develop a weak closed 850-hPa cyclone in the lee of the mountains (not shown), which is consistent with the evolution of Alberta Clippers shown by Thomas and Martin (2007).

In contrast to the zonally progressive storms impacting Canada, the composite mean storm associated with strong ascent over the Intermountain West develops as a diffluent trough digging south from the Pacific Northwest, and then moves inland across northern California, Nevada, and Utah before continuing across the Rocky Mountains (Fig. 6c). This evolution is strikingly similar to that of the Tax Day Storm (section 3a) and is consistent with the experience of operational forecasters. As the composite system crosses Nevada, the accumulated ascent tends to bifurcate into a northern and southern branch. The northern branch is more progressive, while the southern ascent lobe moves meridionally eventually contributing to the regional maximum over Arizona. This ascent splitting is a common feature of storms moving across the Intermountain West and appears in both Figs. 4 and 5a as minima in ascent over northeastern New Mexico.

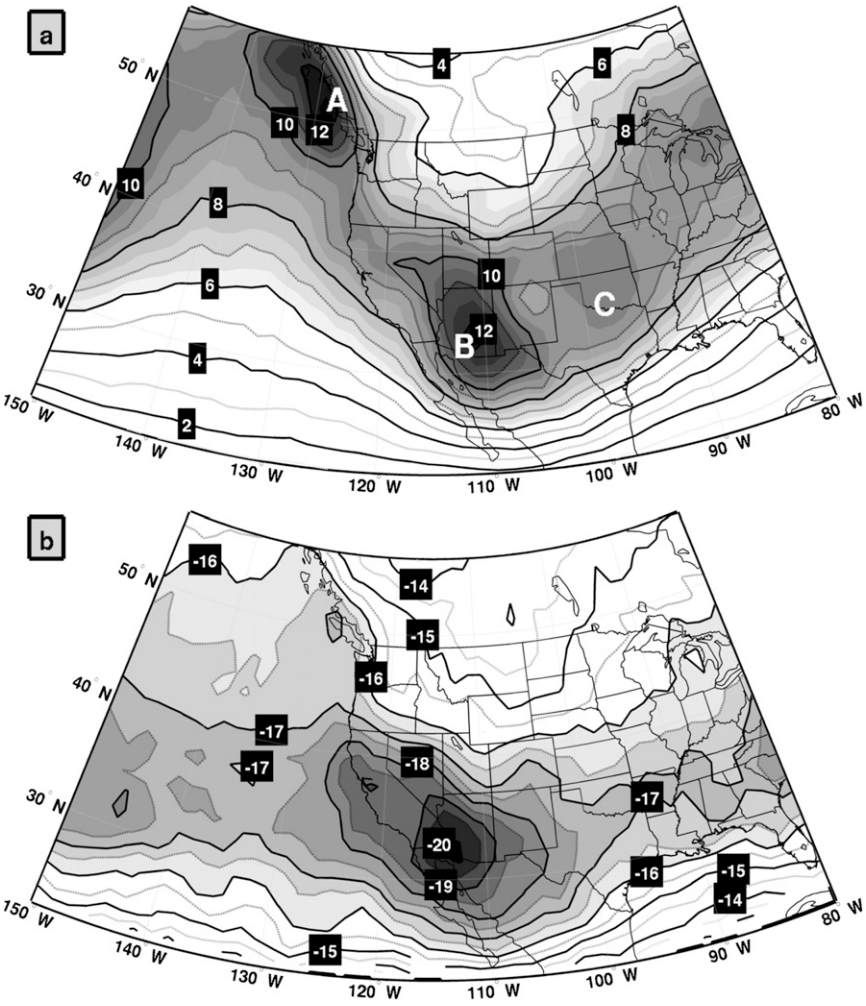

FIG. 5. (a) As in Fig. 4, but for climatological mean frequency of occurrence f. The dashed contour interval is every 1% with solid contours every 2% and shading for values greater than 6% to emphasize regions within the primary storm track. (b) As in Fig. 4, but for climatological mean ascent magnitude per ascent event, $\overline{\omega^*}$. The dashed contours every 0.5 cPa s^{-1}, solid contour every 1 cPa s^{-1}, and shading for values less than -16 cPa s^{-1}.

The composite Arizona storm system is initially similar to the mean intermountain storm, but becomes increasingly elongated in time as the upstream ridge amplifies (Fig. 6d). The attendant increase of planetary vorticity advection into the downstream trough causes it to dig to the south and slow its zonal propagation. This slowing allows the ridge to impinge upon the trough, collapsing the zonal wavelength, and eventually leading to the formation of a closed midtropospheric cyclone over Arizona. Ascent is strongest just prior to the formation of the closed circulation and diminishes rapidly thereafter as the storm becomes equivalent barotropic, fills, and lifts to the northeast as an open wave.

That the composite Arizona storm system forms a closed low is not surprising. The southwestern United States is a well-known preferred location for closed midtropospheric cyclones (Bell and Bosart 1989). However, it is notable that the composite ascent event presented here, which uses no strict definition for storm morphology, is nearly identical to the composite evolution of a small number of closed lows shown by Bell and Bosart (1994).

The motions of numerous additional composite storm paths are subjectively summarized in Fig. 7. Storms over the eastern Pacific progress through the climatologically diffluent flow downstream from the exit of the Pacific jet: southwest to northeast in the Gulf of Alaska, zonally in the east central Pacific, and slightly northwest to southeast over the southern Pacific. As in Figs. 6c,d, the mean storm motion near the U.S. West Coast shifts

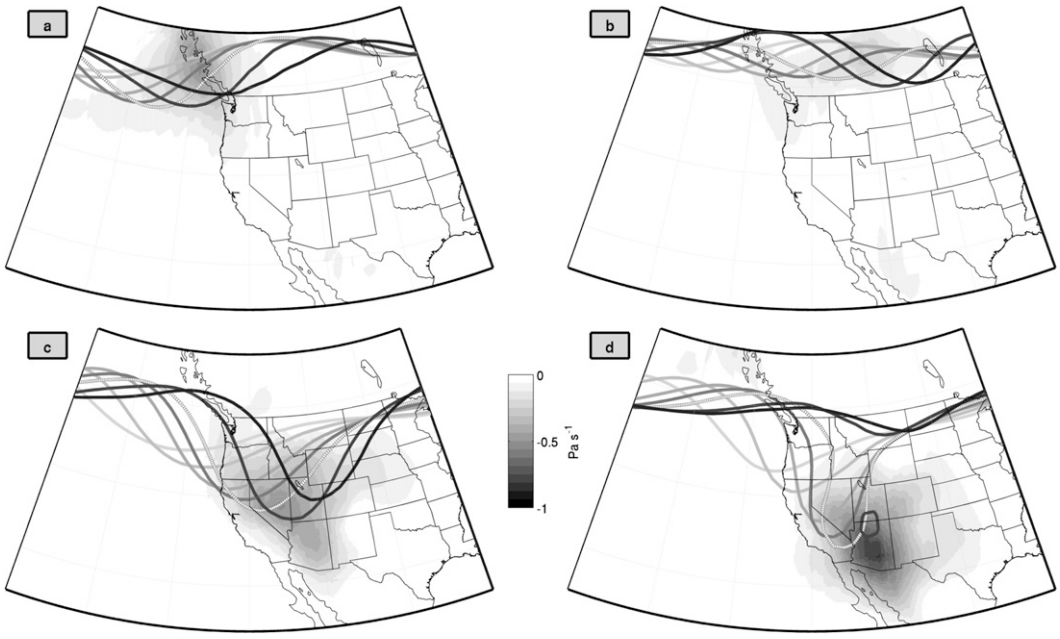

FIG. 6. Composite of 105 cases of strong ascent over: (a) coastal British Columbia, (b) southern Canada, (c) the Intermountain West, and (d) the southwestern United States. Gray shading (according to color bar) indicates the storm total accumulated ascent from $t - 36$ h through $t + 24$ h. Increasingly darker lines indicate the position of the 5400-m [5500 m in (c),(d)], 500-hPa geopotential height contour as a function of composite time ($t = -36$, -24, -12, -6, 0, $+12$, and $+36$ h). The $t = 0$ h contour is emphasized with white dashes.

toward the south. Storms in this region moving south of ~40°N preferentially continue toward the Arizona ascent maximum, whereas storms remaining north of this latitude tend to lift to the northeast across the continental divide. The Arizona storms eventually curve to the northeast passing south of the highest portions of the Rocky Mountains, which are found in central Colorado. To the east of the Rockies, the composite mean storms move rapidly downstream along a predominantly northeasterly path toward the Great Lakes.

In summary, storms with strong ascent across the Canadian provinces develop as low-amplitude zonally propagating troughs moving through the mean ridge, whereas storms bringing ascent to the western United States evolve

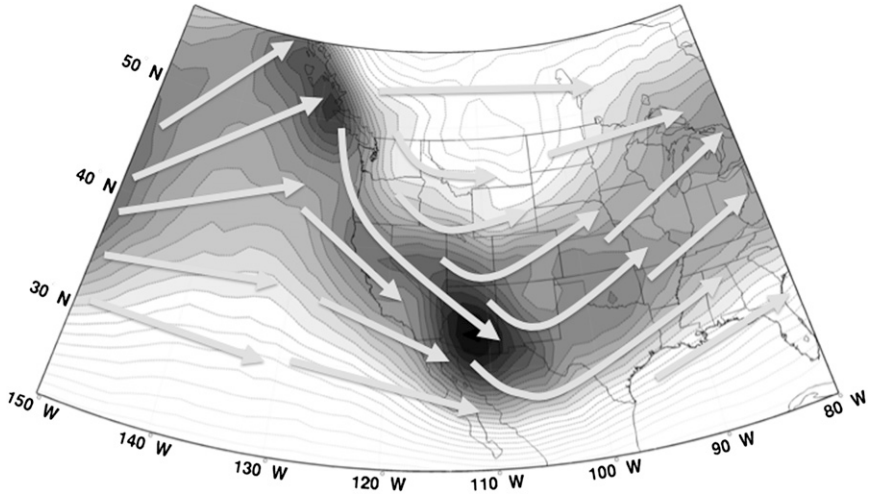

FIG. 7. Conceptual summary of composite storm trajectories. The shading indicates the climatological mean ascent as in Fig. 4.

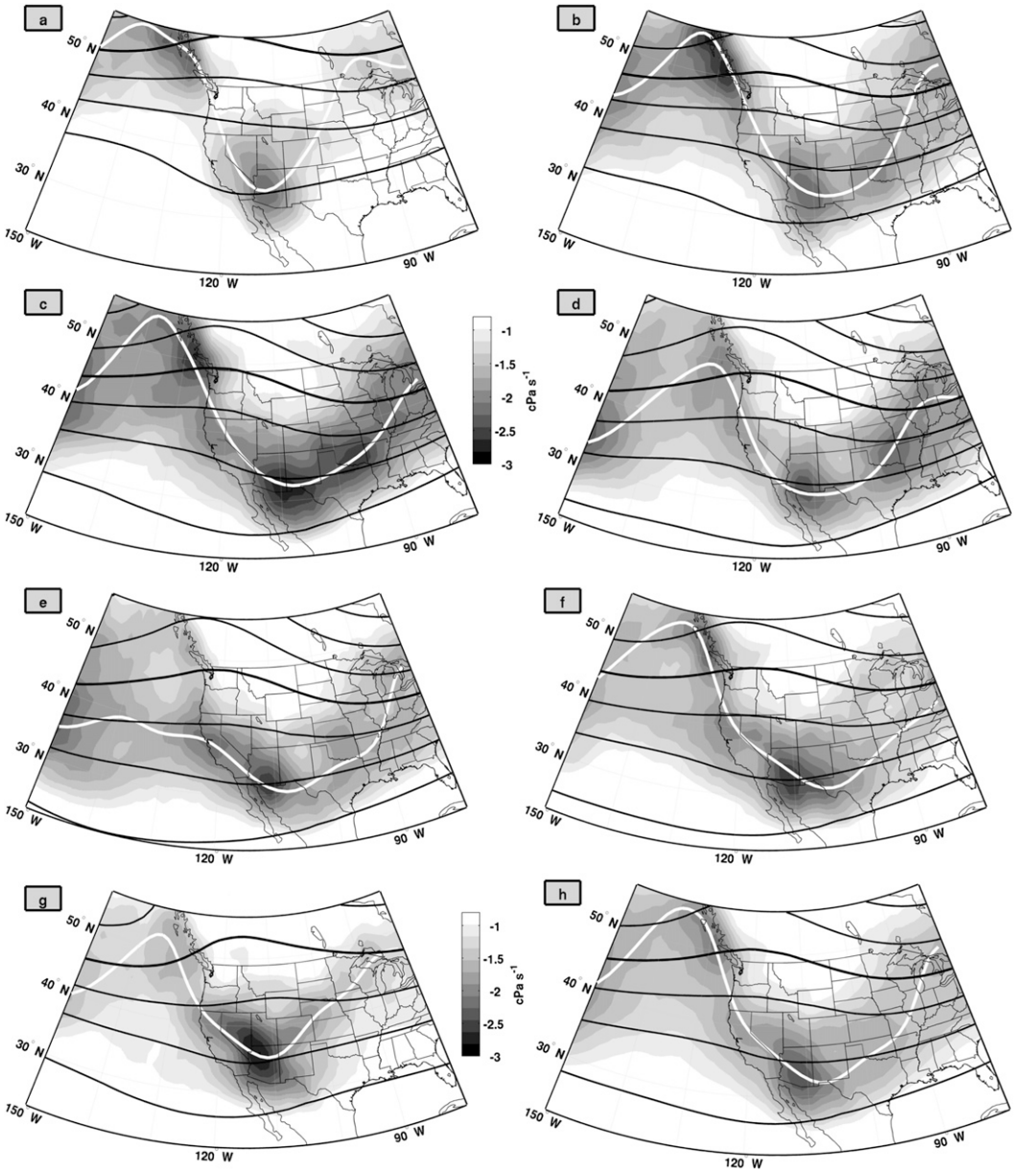

FIG. 8. As in Fig. 4, but for climatological monthly mean synoptic-scale ascent during (a)–(g) October–April.

as digging longwave troughs supplant the climatologically diffluent flow across the region. These two storm tracks do not necessarily occur simultaneously, but rather reflect strong ascent resulting from two distinct types of planetary–synoptic-scale interactions.

d. Seasonality

The seasonal cycle in synoptic-scale ascent exhibits pronounced changes in the amplification and intensity of the sinusoidal storm-track pattern (Fig. 8). These changes occur in concert with seasonal changes in the planetary circulation. As with the climatological mean (Fig. 4), the smoothed centroid of the monthly mean ascent is shown in each panel of Fig. 8 by the heavy solid line, but should not be construed as the mean paths of individual storms during those months. Rather, regionally specific storm dynamics can be inferred similar to those of the composite storm morphologies in the previous section.

During October, ascent is frequent and intense along northern coastal BC upstream from the mean ridge (Fig. 8a). The impact of frequent cutoff lows (Bell and Bosart 1989) over the southwestern United States is apparent in the isolated ascent maximum over Arizona. By November, both the mean height gradient and the mean ascent are

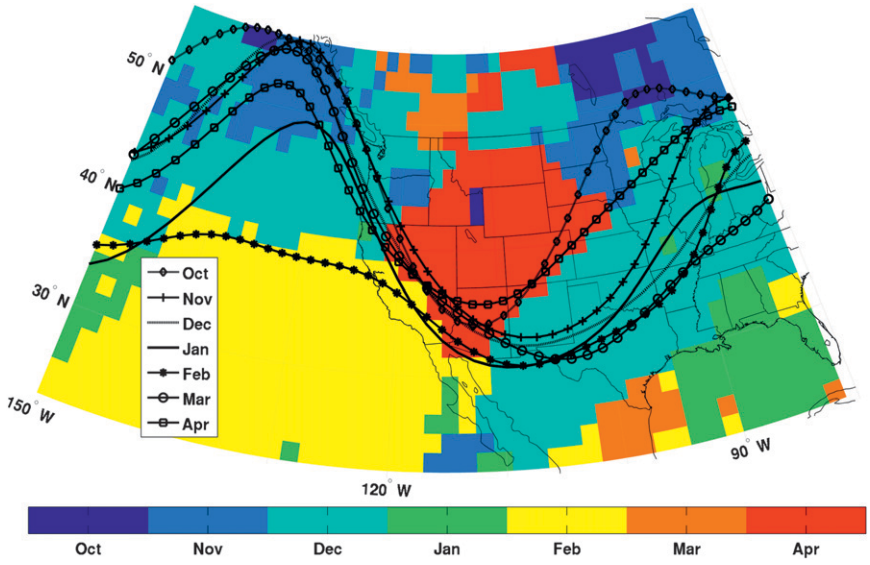

FIG. 9. Calendar month of largest mean synoptic-scale ascent (color shading). The monthly mean storm-track centers are shown for reference.

everywhere enhanced with storms becoming especially more frequent and intense throughout the Pacific Northwest (Fig. 8b). For the domain as a whole, ascent is most intense during December, particularly downstream of the continental divide and proximal to the tertiary maxima (C in Fig. 4) over Oklahoma (Fig. 8c).

Weakening during January of the planetary-scale ridge over western North America leads to diminished ascent in the Pacific Northwest (Fig. 8d). By February, the primary storm track is no longer an amplified sinusoid and instead extends zonally along 40°N across the eastern Pacific Ocean into California (Fig. 8e) although some storms continue to impact coastal BC during this month. The propensity for cutoff lows as well as progressive troughs over the southwestern United States is most pronounced during April (Fig. 8g) and the ascent maximum in this area reaches its largest magnitude of the cool season.

The geographic distribution of the month of maximum climatological ascent (Fig. 9) yields coherent regional patterns consistent with the seasonal progression of the planetary-scale circulation. Ascent along the western seaboard of North America reaches its peak predominantly during November, December, and February as one moves from north to south. In contrast, the largest ascent over much of the Intermountain West and portions of the northern plains tends to take place during April (red shading in Fig. 9). The Sierra Nevada and Cascade mountain ranges (which are oriented roughly north to south through California, Oregon, and Washington) separate the fall-to-winter seasonal progression in ascent over the near-coastal areas from the spring maximum across interior regions. The April ascent maximum is also consistent with the increasing frequency of intermountain cyclones and cyclogenesis (Reitan 1974; Jeglum et al. 2010). Portions of the Canadian Rockies and adjacent regions in Montana and Idaho experience their maximum synoptic-scale ascent during March while the swath of the eastern half of the domain within the primary storm track tends to have a December maximum. Many of these seasonal storm-track features are also apparent in the phase of the annual harmonic of precipitation shown by Hsu and Wallace (1976).

e. *Interannual variability*

Interannual variations in cool season synoptic-scale ascent are identified using principal component analysis (PCA; Horel 1981; Wettstein and Wallace 2010). The PCA is performed on the correlation matrix, whose elements are the correlations between the time series of standardized ascent anomalies for every possible pair of grid points. Because of the relatively small number of years in this study, we use a bootstrapping technique to resample with replacement the years employed in the correlation matrix, although the key results discussed here are not constrained by the sample size. The first principal component (PC-1), derived as the mean leading principal component of 1000 bootstrapped cases, explains one-third (33%) of the total variance. The associated spatial pattern of PC-1 (Fig. 10) indicates that during years when PC-1 is positive (negative), ascent is enhanced generally to the south (north) of the climatological mean

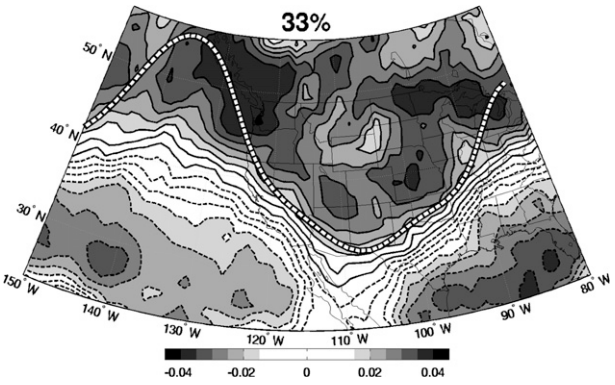

FIG. 10. First principal component (PC-1) loading pattern of interannual variations of synoptic-scale ascent during the cool seasons (October–April) 1989–2010. The contour interval is 0.005 (unitless) with solid (dashed) contours for positive (negative). The explained variance is displayed at the top and the heavy white dashed line shows the climatological mean position of the primary storm track.

position of the storm track. The time series of PC-1 (Fig. 11) indicates that the cool seasons of 1998 and 2010 (1999, 2007, and 2008) correspond to the positive (negative) phase, with increased ascent in the southern sectors of the domain particularly evident during 2010.

The cool season standardized anomaly time series of the multivariate El Niño index (MEI; Wolter and Timlin 1998) is used to demonstrate the connection between the interannual variations in ascent and changes in the planetary-scale circulation forced by variations in equatorial Pacific sea surface temperatures (Fig. 11). The two time series share roughly 44% of their variance in common indicating that El Niño (La Niña) seasons favor enhanced synoptic-scale ascent in the southern (northern) areas of the domain. Composites of ascent during the El Niño seasons of 1992, 1998, and 2010 are compared in Fig. 12 to those during the La Niña seasons of 1999, 2000, and 2008. Consistent with many prior studies of relationships between precipitation and ENSO (Dettinger et al. 1998; Myoung and Deng 2009), enhanced ascent and a more zonal storm track across the southwestern United States is evident in the El Niño seasons, while greater ascent is evident over British Columbia and the Pacific Northwest during the La Niña seasons.

4. Summary and discussion

a. Summary

The AB omega dynamical framework of Davies-Jones (1991) is used to diagnose synoptic-scale vertical motions. This dynamically filtered approach adeptly identifies regions of synoptic-scale ascent in the ERA-Interim, while reducing the impact of poorly resolved mesoscale circulations found in regions of complex terrain. The case study of the Tax Day Storm indicates that synoptic-scale ascent provides an objective and physically meaningful measure of storm location and intensity. The use of an event parameter β defines a storm

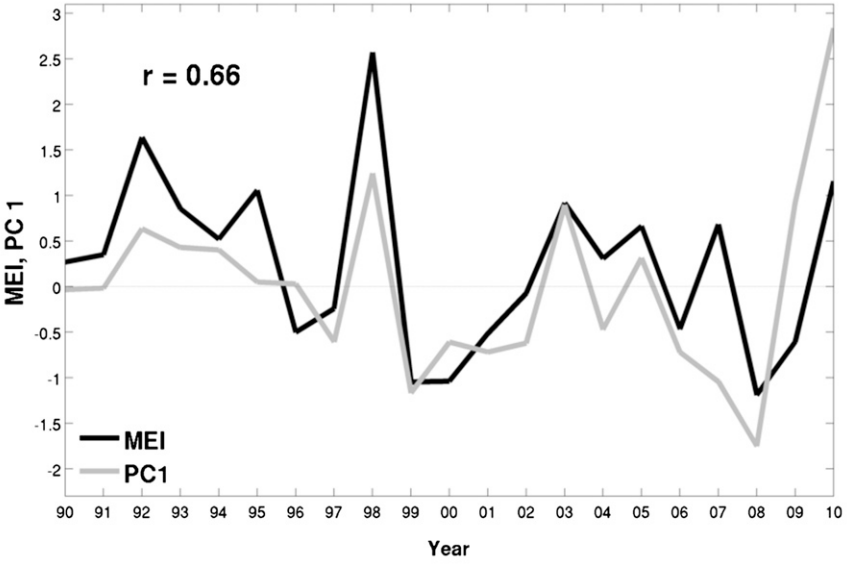

FIG. 11. PC-1 time series and the MEI. Both time series are expressed as standardized anomalies. The Pearson correlation coefficient (*r*) between them is displayed in the top-left corner.

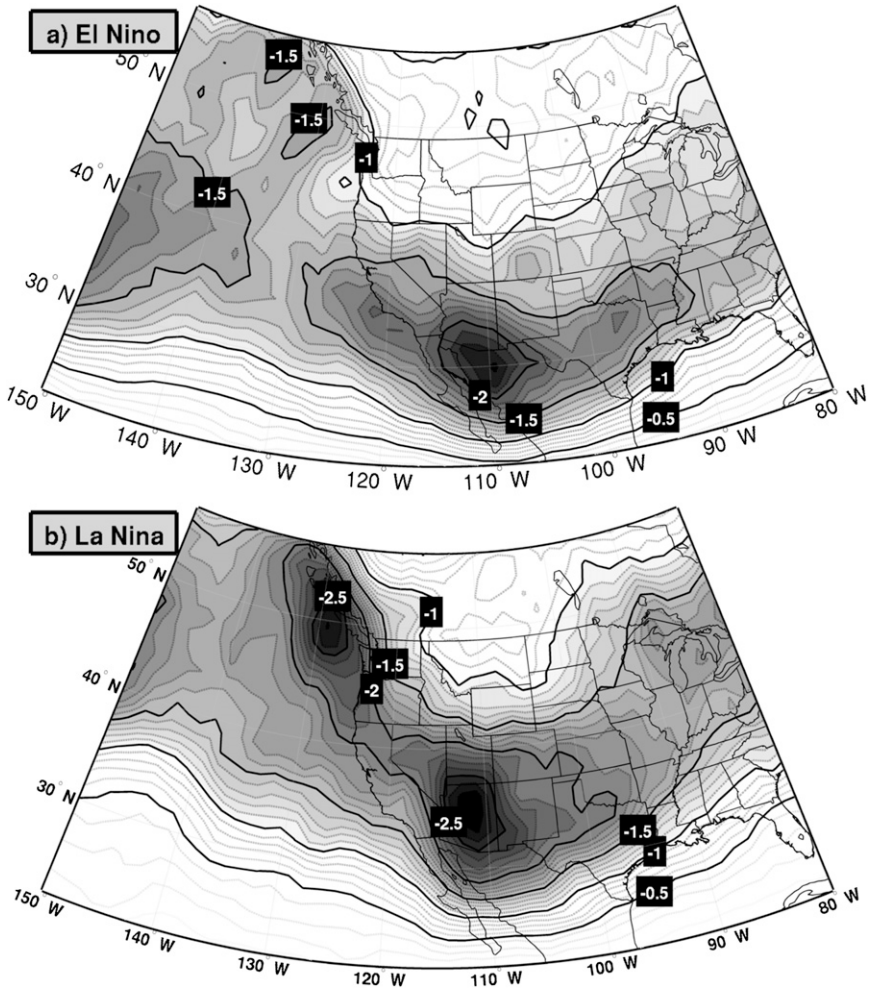

FIG. 12. Composite synoptic-scale ascent for (a) El Niño winters (1992, 1998, and 2010) and (b) La Niña winters (1999, 2000, and 2008). The dashed contours are every 0.1 cPa s^{-1}, solid contours are every 0.5 cPa s^{-1}, and shading is for values less than -1 cPa s^{-1}.

footprint within which the generation of clouds and precipitation as well as changes in the distribution of mass and vorticity accompany strong synoptic-scale ascent. The storm footprint can subsequently be applied to develop storm statistics on time scales from individual storms to long-term climatological means. Its use avoids the need for a rigid morphological storm definition (e.g., closed contours) or bandpass filtering on particular temporal scales that may constrain the features contributing to the storm-track climatology.

The resulting 21-yr cool season climatological distribution of synoptic-scale ascent is found to be an amplified sinusoidal pathway traversing the domain wherein ascent tends to be greatest upstream of the climatological mean ridge over the Canadian Rockies and downstream of the mean trough over the southwestern United States. A weaker secondary storm track extends zonally eastward from the apex of the mean ridge and across portions the Canadian high plains. Regions of high mean ascent occur as a result of the superposition of the trajectories of individual baroclinic eddies embedded within the planetary circulation. Over western North America these trajectories tend to occur in one of three preferred types of synoptic-planetary wave interactions: 1) low-amplitude zonally progressive troughs impacting coastal BC and southern Canada, 2) digging then lifting longwave troughs moving across the Intermountain West, and 3) cutoff lows forming over the southwestern United States.

The seasonal progression of ascent is also closely tied to changes in the position and strength of the planetary-scale ridge and trough over western North America. Ascent increases from fall through early winter over coastal BC and the Pacific Northwest as the prevailing

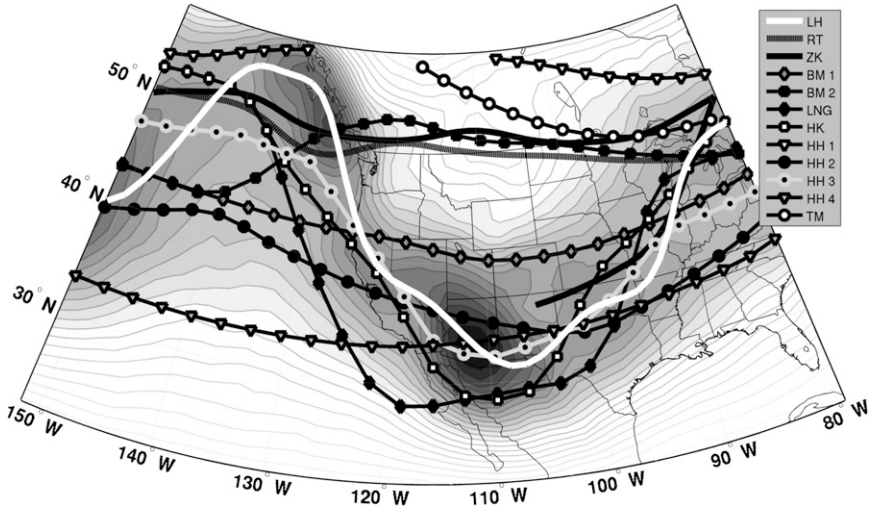

FIG. 13. Climatological mean ascent $\overline{\omega}$ (gray shading according to the color bar) and previous storm-track investigations (assorted lines). Lines are as in Fig. 1 and Table 1, but for the solid white line, which is the center of the climatological ascent storm track, labeled LH (i.e., Lareau and Horel).

southwesterly flow is enhanced. California experiences its peak ascent during February when nearly zonal flow at 40°N allows transient storms to move zonally across the eastern Pacific. A distinct early spring peak in ascent is evident over much of the interior western United States.

Year-to-year variations in synoptic-scale ascent suggest that the amplitude of the sinusoidal storm track peaks during La Niña years and flattens during El Niño winters. Hence, greater ascent across the southwestern United States (Pacific Northwest) is common during El Niño (La Niña) episodes. These interannual variations are consistent with many previous investigations of precipitation variability across the western United States (Changnon et al. 1993; Cayan 1996; Dettinger et al. 1998; Cayan et al. 1999; Myoung and Deng 2009).

b. Discussion

Figure 13 combines Figs. 1 and 4 to summarize our results in the context of prior work. Areas of high climatological mean ascent tend to define an enveloping band within which the majority of previous investigations have found storm tracks to reside. Not surprisingly, the primary sinusoidal ascent storm track coincides most closely with prior studies using midtropospheric metrics (e.g., the climatology of cyclonic relative vorticity at 500 hPa; HK02; solid line with white squares, Fig. 13). In their climatology, a similar curving storm track is evident that extends slightly farther south into northern Mexico than its ascent counterpart. Interestingly, our peak ascent pathway is systematically displaced to the east of the core of the HK02 vorticity storm track, which reflects that ascent arising because of differential absolute vorticity advection maximizes downstream of the location of vorticity centers (Trenberth 1978). Our results are likewise related to the climatology of midtropospheric mobile troughs presented by Lefevre and Nielsen-Gammon (1995; solid line with black diamonds, Fig. 13) and the upper-tropospheric track density for 250-hPa cyclonic relative vorticity (HH02, gray line with black circles, Fig. 13). However, the HH02 bandpass variance of 500-hPa omega (solid line with black circles, Fig. 13) does not correspond as closely to the results in this study.

While both synoptic-scale rising motion and the occurrence of midtropospheric closed cyclones peak over Arizona (Klein et al. 1968; Bell and Bosart 1989, 1994), there is no accompanying climatological maximum in cool season precipitation for this region. This result is notable because numerous studies (Joly et al. 1997; Kocin and Uccellini 2004; Martin 2007) establish a causal chain between upper-level troughs, rising motion, mobile surface cyclones, and sensible weather, such as precipitation. The ascent maximum along the British Columbia coast (A in Fig. 4) fits this conceptual model quite well, where ascent leads to saturation and the generation of precipitation. However, it is apparent that the generally low relative humidity over Arizona acts to limit production of precipitation even in the presence of robust ascent. To confirm this basic result, composites of relative humidity at times of strong synoptic-scale ascent over Arizona were developed (not shown). Despite vigorous rising motion in the composite storm, the relative humidity throughout most of the tropospheric column coincident with updrafts remained below 50%, making precipitation, and even deep clouds, unlikely. It is not surprising then that Rose

and Lin (2003) found very low (high) temporal correlations between the precipitation rate and 700-hPa ascent near the northern Gulf of California (British Columbia).

Despite our explicit assumption that vertical motions are absent below 850 hPa, the ascent "envelope" in Fig. 13 is clearly inclusive of near-surface cyclone climatologies. The weak northern ascent storm track that extends across southern Canada closely corresponds to the cyclone tracks of Reitan (1974) and Zishka and Smith (1980) as well as the preferred path of Alberta Clippers (Thomas and Martin 2007). Across the Intermountain West and downstream of the Rocky Mountains, the multiple cyclone occurrence maxima of Jeglum et al. (2010) and the well-documented Colorado lee cyclogenesis maximum (Petterssen 1956; Zishka and Smith 1980; Smith 1986; Hobbs et al. 1996) are also found beneath regions of high mean ascent. These similarities emphasize the dynamical coupling of increasing vertical motions aloft with the spin up of near-surface relative vorticity through column stretching, which may be especially pronounced when an upper-level baroclinic wave surmounts a lee trough.

c. Future work

We anticipate extending the methodology of this study in a number of directions. For example, in order to better understand the role of synoptic-scale storms on precipitation variability across western North America we hope to use the definition of a storm footprint to partition the region's precipitation into components associated with synoptic-scale ascent and mesoscale orographic forcing. Meanwhile, we intend to apply a "height attributable" version of the AB omega equation (Clough et al. 1996; Deveson et al. 2002) to assess the climatology of dynamical forcing mechanisms over the global domain. This global perspective on storm tracks may also be useful in assessing changes in the location, intensity, and variability of storms in simulated present and future climates such as those shown by Ulbrich et al. (2008).

Acknowledgments. The authors wish to thank Dr. Courtenay Strong for useful contributions in the statistical framing of this study. We also thank Dr. Jim Steenburgh for his insights and recommendations. This research was supported by Rio Tinto Copper as well as by the National Oceanic and Atmospheric Administration under Grants NA07NWS468003 and NA10NWS468005 as part of the CSTAR program.

REFERENCES

Athanasiadis, P. J., J. M. Wallace, and J. J. Wettstein, 2010: Patterns of wintertime jet stream variability and their relation to the storm tracks. *J. Atmos. Sci.,* **67,** 1361–1381.

Bell, G. D., and L. F. Bosart, 1989: A 15-year climatology of Northern Hemisphere 500 mb closed cyclone and anticyclone centers. *Mon. Wea. Rev.,* **117,** 2142–2164.

——, and ——, 1994: Midtropospheric closed cyclone formation over the southwestern United States, the eastern United States, and the Alps. *Mon. Wea. Rev.,* **122,** 791–813.

Bengtsson, L., K. I. Hodges, and E. Roeckner, 2006: Storm tracks and climate change. *J. Climate,* **19,** 3518–3543.

Blackmon, M. L., 1976: A climatological spectral study of the 500 mb geopotential height of the Northern Hemisphere. *J. Atmos. Sci.,* **33,** 1607–1623.

Brayshaw, D. J., B. J. Hoskins, and M. Blackburn, 2009: The basic ingredients of the North Atlantic storm track. Part I: Land-sea contrast and orography. *J. Atmos. Sci.,* **66,** 2539–2558.

Cayan, D. R., 1996: Interannual climate variability and snowpack in the western United States. *J. Climate,* **9,** 928–948.

——, D. H. Peterson, and L. Riddle, 1999: ENSO and hydrologic extremes in the western United States. *J. Climate,* **12,** 2881–2893.

Changnon, D., T. B. McKee, and N. J. Doesken, 1993: Annual snowpack patterns across the Rockies: Long-term trends and associated 500-mb synoptic patterns. *Mon. Wea. Rev.,* **121,** 633–647.

Clough, S. A., C. S. A. Davitt, and A. J. Thorpe, 1996: Attribution concepts applied to the omega equation. *Quart. J. Roy. Meteor. Soc.,* **122,** 1943–1962.

Davies-Jones, R., 1991: The frontogenetical forcing of secondary circulations. Part I: The duality and generalization of the Q vector. *J. Atmos. Sci.,* **48,** 497–509.

——, 2009: The frontogenetical forcing of secondary circulations. Part II: Properties of Q vectors in exact linear solutions. *J. Atmos. Sci.,* **66,** 244–260.

Davis, C. A., 1997: The modification of baroclinic waves by the Rocky Mountains. *J. Atmos. Sci.,* **54,** 848–868.

——, and M. T. Stoelinga, 1999: Interpretation of the effect of mountains on synoptic-scale baroclinic waves. *J. Atmos. Sci.,* **56,** 3303–3320.

Dee, D. P., and Coauthors, 2011: The ERA-Interim reanalysis: Configuration and performance of the data assimilation system. *Quart. J. Roy. Meteor. Soc.,* **137,** 553–597.

Dettinger, M. D., D. R. Cayan, H. F. Diaz, and D. M. Meko, 1998: North–south precipitation patterns in western North America on interannual-to-decadal time scales. *J. Climate,* **11,** 3095–3111.

Deveson, A. C. L., K. A. Browning, and T. D. Hewson, 2002: A classification of FASTEX cyclones using a height-attributable quasi-geostrophic vertical-motion diagnostic. *Quart. J. Roy. Meteor. Soc.,* **128,** 93–117.

Durran, D. R., and L. W. Snellman, 1987: The diagnosis of synoptic-scale vertical motion in an operational environment. *Wea. Forecasting,* **2,** 17–31.

Elbern, H., J. Hendricks, and A. Ebel, 1998: A climatology of tropopause folds by global analysis. *Theor. Appl. Climatol.,* **59,** 181–200.

Glickman, T. S., 2000: *Glossary of Meteorology*. 2nd ed. Amer. Meteor. Soc., 855 pp.

Hakim, G. J., 2000: Climatology of coherent structures on the extratropical tropopause. *Mon. Wea. Rev.,* **128,** 385–406.

Hobbs, P. V., J. D. Locatelli, and J. E. Martin, 1996: A new conceptual model for cyclones generated in the lee of the Rocky Mountains. *Bull. Amer. Meteor. Soc.,* **77,** 1169–1178.

Holton, J. R., 2004: *An Introduction to Dynamic Meteorology*. 4th ed. Elsevier, 535 pp.

Horel, J. D., 1981: A rotated principal component analysis of the interannual variability of the Northern Hemisphere 500 mb height field. *Mon. Wea. Rev.,* **109,** 2080–2092.

Hoskins, B. J., and M. A. Pedder, 1980: The diagnosis of middle latitude synoptic development. *Quart. J. Roy. Meteor. Soc.,* **106,** 707–719.

——, and K. I. Hodges, 2002: New perspectives on the Northern Hemisphere winter storm tracks. *J. Atmos. Sci.,* **59,** 1041–1061.

——, I. Draghici, and H. C. Davies, 1978: A new look at the ω-equation. *Quart. J. Roy. Meteor. Soc.,* **104,** 31–38.

Hsu, C.-P. F., and J. M. Wallace, 1976: The global distribution of the annual and semiannual cycles in precipitation. *Mon. Wea. Rev.,* **104,** 1093–1101.

Jeglum, M. E., W. J. Steenburgh, T. P. Lee, and L. F. Bosart, 2010: Multi-reanalysis climatology of intermountain cyclones. *Mon. Wea. Rev.,* **138,** 4035–4053.

Joly, A., and Coauthors, 1997: The Fronts and Atlantic Storm-Track Experiment (FASTEX): Scientific objectives and experimental design. *Bull. Amer. Meteor. Soc.,* **78,** 1917–1940.

Keyser, D., M. J. Reeder, and R. J. Reed, 1988: A generalization of Petterssen's frontogenesis function and its relation to the forcing of vertical motion. *Mon. Wea. Rev.,* **116,** 762–781.

Klein, W. H., 1957: Principal tracks and mean frequencies of cyclones and anticyclones in the Northern Hemisphere. Weather Bureau Research Paper 40, 60 pp.

——, D. L. Jorgensen, and A. F. Korte, 1968: Relation between upper air lows and winter precipitation in the western plateau states. *Mon. Wea. Rev.,* **96,** 162–168.

Kocin, P. J., and L. W. Uccellini, 2004: *Northeast Snowstorms*. Vols. 1 and 2, *Meteor. Monogr.,* No. 54, Amer. Meteor. Soc., 818 pp.

Krishnamurti, T. N., and L. Bounoua, 1996: *An Introduction to Numerical Weather Prediction Techniques*. CRC Press, 293 pp.

Lau, N.-C., 1988: Variability of the observed midlatitude storm tracks in relation to low-frequency changes in the circulation pattern. *J. Atmos. Sci.,* **45,** 2718–2743.

Lefevre, R. J., and J. W. Nielsen-Gammon, 1995: An objective climatology of mobile troughs in the Northern Hemisphere. *Tellus,* **47A,** 638–655.

Martin, J. E., 2006: *Mid-Latitude Atmospheric Dynamics: A First Course*. Wiley, 324 pp.

——, 2007: Lower-tropospheric height tendencies associated with the shearwise and transverse components of quasigeostrophic vertical motion. *Mon. Wea. Rev.,* **135,** 2803–2809.

Mote, P. W., 2006: Climate-driven variability and trends in mountain snowpack in western North America. *J. Climate,* **19,** 6209–6220.

——, A. F. Hamlet, M. P. Clark, and D. P. Lettenmaier, 2005: Declining mountain snowpack in western North America. *Bull. Amer. Meteor. Soc.,* **86,** 39–49.

Myoung, B., and Y. Deng, 2009: Interannual variability of the cyclonic activity along the U.S. Pacific coast: Influences on the characteristics of winter precipitation in the western United States. *J. Climate,* **22,** 5732–5747.

Petterssen, S., 1956: *Weather Analysis and Forecasting*. Vol. 1. 2nd ed. McGraw-Hill, 428 pp.

Pierce, D. W., and Coauthors, 2008: Attribution of declining western U.S. snowpack to human effects. *J. Climate,* **21,** 6425–6444.

Raible, C. C., P. M. Dellat-Marta, C. Schwierz, H. Wernli, and R. Blender, 2008: Northern Hemisphere extratropical cyclones: A comparison of detection and tracking methods and different reanalyses. *Mon. Wea. Rev.,* **136,** 880–897.

Reitan, C. H., 1974: Frequencies of cyclones and cyclogenesis for North America, 1951–1970. *Mon. Wea. Rev.,* **102,** 861–868.

Rose, B. E. J., and C. A. Lin, 2003: Precipitation from vertical motion: A statistical diagnostic scheme. *Int. J. Climatol.,* **23,** 903–919.

Serreze, M. C., M. P. Clark, R. L. Armstrong, D. A. McGinnis, and R. S. Puwarty, 1996: Characteristics o the western U.S. snowpack from SNOTEL data. *Water Resour. Res.,* **35,** 2145–2160.

Sickmöller, M., R. Blender, and K. Fraedrich, 2000: Observed winter cyclone tracks in the northern hemisphere in re-analysed ECMWF data. *Quart. J. Roy. Meteor. Soc.,* **126,** 591–620.

Smith, R. B., 1986: Further development of a theory of lee cyclogenesis. *J. Atmos. Sci.,* **43,** 1582–1602.

Thomas, B. C., and J. E. Martin, 2007: A synoptic climatology and composite analysis of the Alberta Clipper. *Wea. Forecasting,* **22,** 315–333.

Trenberth, K. E., 1978: On the interpretation of the diagnostic quasi-geostrophic omega equation. *Mon. Wea. Rev.,* **106,** 131–137.

Ulbrich, U., J. G. Pinto, H. Kupfer, G. C. Leckebusch, T. Spangehl, and M. Reyers, 2008: Changing Northern Hemisphere storm tracks in an ensemble of IPCC climate change simulations. *J. Climate,* **21,** 1669–1679.

Wernli, H., and C. Schwierz, 2006: Surface cyclones in the ERA-40 dataset (1958–2001). Part I: Novel identification method and global climatology. *J. Atmos. Sci.,* **63,** 2486–2507.

West, G. L., and W. J. Steenburgh, 2010: Life cycle and mesoscale frontal structure of an intermountain cyclone. *Mon. Wea. Rev.,* **138,** 2528–2545.

Wettstein, J. J., and J. M. Wallace, 2010: Observed patterns of month-to-month storm-track variability and their relationship to the background flow. *J. Atmos. Sci.,* **67,** 1420–1437.

Whittaker, L. M., and L. H. Horn, 1981: Geographical and seasonal distribution of North American cyclogenesis, 1958–1977. *Mon. Wea. Rev.,* **109,** 2312–2322.

Wolter, K., and M. S. Timlin, 1998: Measuring the strength of ENSO events—How does 1997/98 rank? *Weather,* **53,** 315–324.

Zishka, K. M., and P. J. Smith, 1980: The climatology of cyclones and anticyclones over North America and surrounding ocean environs for January and July, 1950–77. *Mon. Wea. Rev.,* **108,** 387–401.